ELSEVIER

Journal of Structural Geology 30 (2008) 366–379

JOURNAL OF STRUCTURAL GEOLOGY

www.elsevier.com/locate/jsg

Effect of basal friction on surface and volumetric strain in models of convergent settings measured by laser scanner

Faramarz Nilforoushan [a,*], Hemin A. Koyi [a], Jan O.H. Swantesson [b], Christopher J. Talbot [a]

[a] Department of Earth Sciences, Hans Ramberg Tectonic Laboratory, Uppsala University, Villavegen 16, SE-752 36 Uppsala, Sweden
[b] Department of Physical Geography, Faculty of Technology and Science, Karlstad University, SE-65188 Karlstad, Sweden

Received 20 March 2007; received in revised form 16 September 2007; accepted 21 September 2007
Available online 5 November 2007

Abstract

This paper uses measurements by a high-accuracy laser scanner to investigate the role of basal friction on surface and volumetric strains in sandbox models simulating fold-thrust belts and accretionary wedges. We monitor progressive deformation, wedge growth, and strain distribution in three models with similar initial boundary conditions but with different basal frictions. Our analyses show that, in addition to influencing the kinematics and geometry of model wedges, basal friction also governs both the surface and volumetric strains of the wedge. After 16.3% bulk shortening, the volume decreased $5 \pm 0.5\%$, $9.5 \pm 0.5\%$ and $12.5 \pm 0.5\%$ in the models shortened above low, intermediate and high friction decollements, respectively. Applied to nature, our model results suggest that more compaction and penetrative strain is expected in convergent settings with a high-friction decollement than those shortened above a low-friction decollement or a weak basal bed (like the salt formation under parts of the Zagros fold-thrust belt). This volume decrease probably reduces the porosity in the deformed lithologies.

Keywords: Analogue modeling; Basal friction; Fold-thrust belt; Volumetric strain; Laser scanning; Zagros

1. Introduction

The formation and evolution of accretionary prisms and fold-thrust belts have been simulated in many analogue models (Davis et al., 1983; Malavieille, 1984; Mulugeta, 1988; Liu et al., 1992; Mulugeta and Koyi, 1992; Calassou et al., 1993; Lallemand et al., 1994; Gutscher et al., 1996, 1998; Koyi, 1995, 1997; Nieuwland et al., 2000; Costa and Vendeville, 2002; Lohrmann et al., 2003; Buiter and Schreurs, 2006; Schreurs et al., 2006). Friction along the basal sliding surface (detachment; decollement or sole thrust) is one of the main parameters that influence thin-skin deformation in convergent settings (fold-thrust belts or accretionary wedges) (e.g.; Davis et al., 1983; Dahlen et al., 1984; Davis and Engelder, 1985; Mulugeta, 1988; Cotton and Koyi, 2000; Agarwal and Agrawal, 2002; Bahroudi and Koyi, 2003; Ford, 2004; Koyi and Cotton, 2004; Bonini, 2007). Different decollement frictions yield different wedge geometries and kinematics. Over-pressurization or hydration of sediments adjoining natural decollements reduces the frictional resistance and thereby affects the overlying wedges (e.g. Mourgues and Cobbold, 2006). High intraplate seismicity has also directly been correlated with high basal friction (Koyi et al., 2000; Huene and Ranero, 2003). Schott and Koyi (2001) and Maillot and Koyi (2006) discuss theoretical inferences of basal friction from the geometry of a fold-thrust belt. All these studies emphasize the role of basal friction in influencing the kinematics and geometry of the wedge as well as deformation mechanisms from intergranular scales to plate margins.

Earlier analogue models monitored the evolution of the geometry and internal structures of accretionary prisms and fold-thrust belts mainly from the top surface or in 3D using cross-sections parallel to the shortening direction (e.g. Mulugeta and Koyi, 1987, 1992; Mulugeta, 1988; Huiqui et al., 1992) or X-ray tomography (Colletta et al., 1991; Schreurs et al., 2001).

* Corresponding author. Present address: Geodynamic Department, National cartographic Center, PO Box 13185-1684, Meraj Ave, Tehran, Iran. Tel.: +46 18 471 2585; fax: +46 18 471 2591.
E-mail address: faramarz.nilfouroushan@geo.uu.se (F. Nilforoushan).

0191-8141/$ - see front matter © 2007 Elsevier Ltd. All rights reserved.
doi:10.1016/j.jsg.2007.09.013

In an earlier study (Nilforoushan and Koyi, 2007), we estimated and compared the surface strains using digital images of the surface of models shortened above a high frictional and a viscous decollement layer. There, we followed previous studies (e.g., Davis and Engelder, 1985; Cotton and Koyi, 2000; Schreurs et al., 2001) and used a viscous layer to simulate salt or shale (which behaves as a viscous fluid) as a natural low-friction decollement. Nilforoushan and Koyi (2007) quantified different model strain fields above viscous and frictional decollements and compared the results to a natural example. In this study, no viscous layer was used for low-friction model. Instead the sand layers were shortened above a rigid aluminum basement that provided a low basal friction. This was done because a ductile/viscous layer sitting above the basement deforms and its thickness changes during the model shortening. As such, its behavior is different from a rigid low-friction decollement above which only the overburden ''cover sediments'' deforms (e.g. Ford, 2004). In this study, we also use a high-accuracy laser scanner to map the topography of the model surface after shortening increments above low, intermediate and high-friction decollements with similar initial boundary conditions and we then explore the relationship of surface and volumetric strains with basal friction. The laser scanner provided detailed information about the progressive growth of wedges in three different models and enabled highlighting the role of basal friction in the evolution of wedge.

We compare the topographies and tapers of our models with those of a natural convergent zone in SW Iran, namely the Zagros fold-thrust belt where adjoining high and low basal friction wedges are still being built by the convergence of Arabia and Eurasia (e.g. Nilforoushan et al., 2003; Hessami et al., 2006).

2. Model setup and methods

2.1. Model setup

Three models were prepared in this study. Following previous studies, loose sand was used to simulate brittle deformation in cover units in nature (e.g. Davy and Cobbold, 1991; Weijermars et al., 1993; Koyi and Petersen, 1993; Bonini, 2001). The sand used has an internal coefficient of friction of $\mu = 0.57$ (angle of internal friction $\theta = 30^\circ$) measured in the same way as in Maillot and Koyi (2006), a bulk density, $\rho = 1550$ kg/m^3, a cohesive strength, C = 140 Pa and an average grain size of about $\geq$35 μm (Cotton and Koyi, 2000).

Three identical rectangular models consisting of a 25 mm thick layer of loose sand and initial dimensions of 49 × 45 cm were prepared. These models were placed horizontally on an aluminum table representing a rigid flat basement. The only parameter varied in these models was the coefficient of basal friction, which was measured as described in Maillot and Koyi (2006). A new aluminum sheet on the floor of the box was used as a low-friction decollement (basal coefficient of friction $\mu_b = 0.36$, angle of basal friction $\theta = 20^\circ$). The intermediate-friction decollement was a 4 mm thick sheet of wood with a basal coefficient of friction $\mu_b = 0.5$ ($\theta = 27^\circ$). We glued a ca. 1 mm thick layer of loose sand on an aluminum sheet to act as a high-friction ($\mu_b = 0.7$, $\theta = 35^\circ$) decollement (Fig. 2).

A digital camera was mounted 80 cm above the model to take digital images of the surface after each stage (1 cm increment) of thin-skinned shortening. To compare the digital images and study the progressive deformation, we defined a static reference coordinate system where four points were marked on aluminum bars and placed on the side walls at the frontal part of the model and near the surface where no deformation was expected. The coordinates of these control points were used to establish a unique reference coordinate system for all images (for more details, see Nilforoushan and Koyi, 2007). Using these control points, transformation parameters between the initial image of the undeformed surface and subsequent images after increments of deformation could be estimated whenever needed. Having the camera fixed above a stable table meant that the coordinates of the control points remained fixed and ensured that the unique reference frame remained static.

A rectangular grid (12 × 12 mm) was printed on the surface of each model. The corners of this passive grid were coordinated during model shortening and their displacements were used to estimate surface strains (for more details of this method, see Nilforoushan and Koyi, 2007).

A high-accuracy laser scanner (±0.1 mm) (Fig. 1) was mounted above the model on a rigid horizontal frame to measure the lateral and vertical movement of the model surface during each experiment. The four legs of the scanner frame were screwed to the experimental table to ensure that this frame, which provides the coordinate system of the recorded data, remained static during each experiment. In addition to tracking the passive grid corners to monitor horizontal strains, we added some extra control points on the model surface and followed their movements using the laser scanner for volume measurements. As reflections of the laser-beam from the model walls would introduce unavoidable multi-path noise, only the rectangular ABCD area (285 × 338 mm) in Fig. 1 was measured. This was a few centimeters away from the model walls to diminish side effects. The initial location of this scanned area was the same in all three models (Fig. 1). In addition to scanning of the ABCD area, the extra control points along AC and BD forming parallel lines to CD helped to scan surface segments individually to estimate and take into account the volume of material entering the ABCD area (Fig. 1) from the rear of the scanned area.

2.1.1. Laser scanner

The contact-free laser scanner we used was originally designed for detailed mapping of the micro-topography of rock surfaces in the field. Repeated measurements by this machine have successfully monitored the progress of physical weathering on sites with Bronze Age rock carvings in Sweden (Swantesson, 2005, 2006). The laser scanner has also been used to monitor downwearing rates and erosion on rocky coasts in various European countries (Swantesson et al., 2006) and to interpret ancient runic inscriptions that are difficult to read with the naked eye (Swantesson and Gustavson, 2005). The

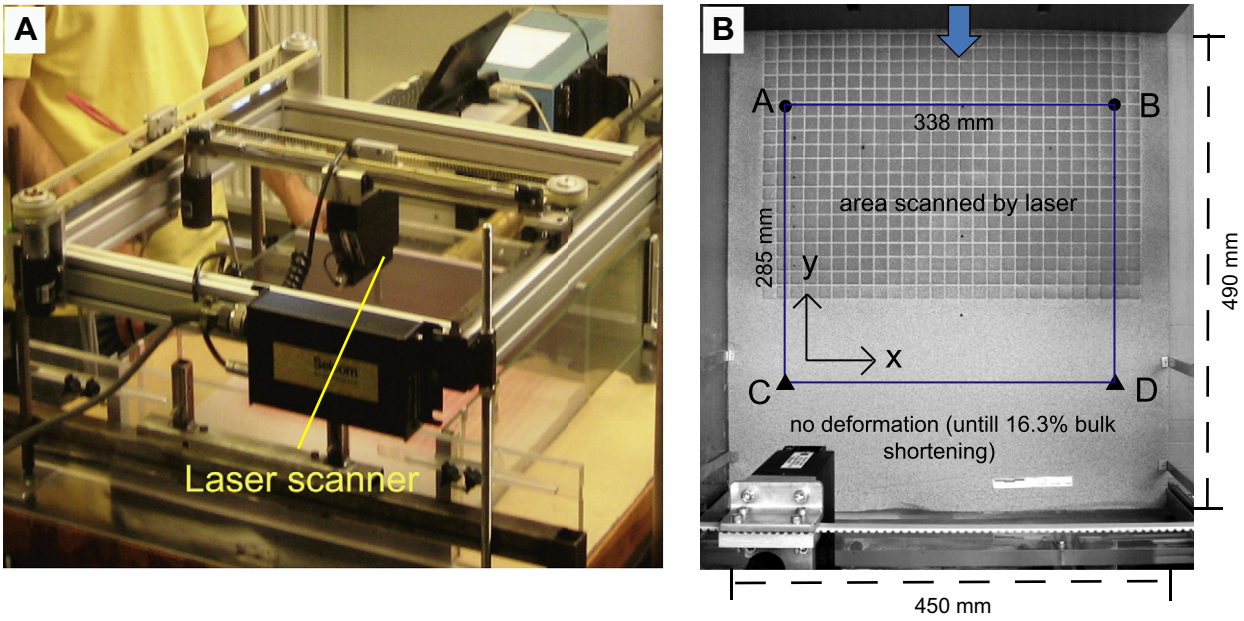

Fig. 1. (A) Model setup including sandbox and laser scanner. (B) Image of initial model surface with regular 12 × 12 mm grid and control points. The line CD at the end of scanned area is static during our experiment and rectangle ABCD is tracked by laser-scanner after each shortening increment. The laser-scanner coordinate system with arbitrary origin C (coordinates $x = 20$ and $y = 50$) is also shown. Thick arrow shows shortening direction.

performance and reliability of the apparatus has thus been thoroughly tested. Technical descriptions of the entire equipment, as well as discussions about the advantages and disadvantages of a so-called triangulation type laser for the study of micro-topography are treated by Williams et al. (2000), Swantesson (2005) and Swantesson et al. (2006).

The basic unit of the micro-mapping device is a commercially available low-power GeAs laser, which emits a beam of red light (wavelength 670 nm). Where the beam hits the surface, it creates a red spot with a diameter of 0.2 mm. A detector mounted at an angle to the laser source focuses the spot on the surface and the height or elevation (z-value) can be recorded with respect to a defined datum. The resolution in the z-direction is 0.025 mm within a height interval of 100 mm and the final accuracy is about 0.1 mm in the field. In the laboratory accuracy can be expected to be somewhat better due to more controlled environmental conditions. Two stepping motors mounted on an aluminum frame moved the laser gauge probe in the x- and y-directions (Fig. 1A) making it possible to scan surfaces of up to 400 × 400 mm. During the scans, data are collected directly on a computer in a regular grid. Maps of the micro-topography, 3D-models and various other types of images are readily obtained directly from the collected data set using a range of software. The problems of using a laser of the triangulation type are well known, notably missing z-values or unwanted reflections near abrupt edges on the measured surface. Since the topography of our sandbox models was fairly smooth we did not encounter these problems. An advantage of a flatbed laser scanner is that all resulting maps and other images are in a true orthogonal projection. No parallax errors can arise, as for example, when a central projection is obtained. Calculations of height differences and, indirectly, volume changes between the consecutive shortening stages of the sandbox models, can thus be made by simple subtractions. There is no need for adjustments and recalculations of data grids that can decrease the accuracy of the final results. The high-accuracy laser measurements of heights in our models allowed us to study vertical changes in the upper surface of each model without disturbing it, and disclosed the presence of inner and outer wedges which is described later.

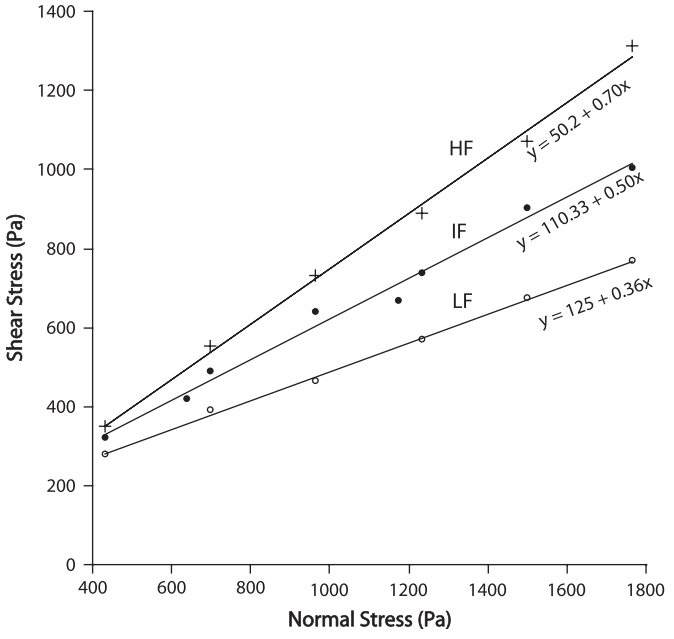

Fig. 2. Shear stress (τ) as a function of normal stress (σ) for three different surfaces used in the models. The three straight lines obtained by linear regression.

2.2. Methods

Three models (low-friction decollement = LF, intermediate-friction decollement = IF and high-friction decollement = HF) were shortened by advancing a rear wall at an average rate of 20 mm/h. The base of the model was scanned before it was filled with sand and compared with scans of the initial and deformed surfaces to estimate the volume of sand in our scanned area after each increment of shortening.

Each model was stopped after every 1 cm of shortening for photography and laser scanning. Keeping the line CD (Fig. 1) near the fixed wall static (up to 16.3% bulk shortening) deformation of the scanned area (ABCD) was followed by tracking the line AB by the laser scanner. After each centimeter of shortening, ABCD was scanned by laser with a spacing of 1 mm along each scan line with a positional accuracy of the XY gantry of ±0.2 mm. Each surface scan took about 2 h.

The coordinates of the extra control points in the scanned area were also tracked individually by the laser-scanner after each stage of shortening. Adding these control points helped to transform the Cartesian coordinate system of the scanner to the coordinate system of the digital images of the model surface.

Due to the dimensions of the scanner frame (400 × 400 mm) and reflections from the rear wall, we could scan only the rectangular area, ABCD, shown in Fig. 1. To avoid the deformation reaching CD, especially for the LF model, the shortening of all three models was stopped after 8 cm (16.3%) of bulk shortening.

3. Results

3.1. Topography

Accurate laser measurements provided high-accuracy 3D data sets of model topographies that recorded the geometric and kinematic evolution of each model as the deformation front advanced. To focus on topographical changes and compare the three experimental thrust wedges, the topography of the initial top surface was measured before deformation and subtracted from the deformed topography. The resulting residual topographies for the three models at the final stage of shortening (16.3% of bulk shortening) were produced and found to relate to the different basal frictions. The residual topographies show that deformation is more diffuse and the topography is lower in the LF model (Fig. 3). The imbricate zone is more localized in IF and HF than in LF. A second imbricate zone developed in the LF model due to the fast advance of the deformation front. In the scanned area (Figs. 1 and 3A), the deformation front (where the surface rises 0.5 mm) advanced mainly parallel to the rear wall with minimal boundary effects. The deformation front advanced to different distances in each model and in the LF model advanced about 1.5 times the distance in the HF model (Figs. 3 and 4).

Model deformation was monitored by scanning the model surface after each 1 cm increment of shortening (Fig. 4). To avoid side effects, topographical profiles parallel to the shortening direction, were extracted from the scans in the middle of each model (Fig. 3). After 1 cm lateral bulk shortening, the surface near AB, at the rear of the models, rose between 0.5 and 2 mm in all three models. The horizontal location of this initial rise in the three models differed by about a few millimeters and was further from the rear wall in the LF model. The rear of the model rose faster in the HF model and continued shortening led to the development of a wedge whose taper grew to a steady angle (Fig. 4). The wedge height increased faster in models with higher basal friction. The maximum wedge heights were 26 mm, 24 mm and 15 mm in the HF, IF and LF models respectively (Figs. 4 and 5).

The advance of deformation fronts in the IF and HF models are similar and show a linear relationship with bulk shortening implying an approximate constant rate of growth (Fig. 5A). In contrast, the deformation front advanced at variable rates in the LF model (Fig. 5A). The wedge heights grew almost linearly and it was similar in the IF and HF models (Fig. 5B). The topographical slope measurements show the self-similar growth of the wedge in IF and HF models (see next section). In the LF model the wedge height grew non-linearly where its height did not grow as fast during the later stages of shortening (Fig. 5B).

3.2. Tapers

Accurate laser monitoring of the upper surface topography during shortening of the LF model shows a wedge with a complex geometry (inner and outer wedges). The two wedges grew simultaneously from the initial stages throughout model shortening. In addition to forming a main wedge (inner wedge with taper T1 in Fig. 4) (as described in e.g. Davis et al., 1983; Dahlen et al., 1984; Dahlen, 1990) a frontal (outer) thin wedge grew (T2) in front of the main wedge at every stage (Fig. 4). T1 and T2 are the topographical slopes of the inner and outer wedges respectively. To measure the taper angles (α) we notice to wedge toes and approximate the slope angle of upper surface topography. For HF and IF, the taper is clear. However, the LF model is not as easy. Therefore, we have followed the growth of the wedge from the beginning and monitored the forward propagation of the wedge toe with the laser scanner. By doing this, we have been able to approximate the geometry and taper of the wedge in the LF model as well.

There is a direct correlation between the taper of T1 and basal friction, i.e. a higher taper angle forms in high-friction models (T1 taper angles α of 9°, 19° and 21° were measured for the models LF, IF and HF, respectively at the final stage of shortening (Fig. 4)). The first taper (T1) is much steeper in the HF and IF models and dominates the final geometry of the wedge (Fig. 4). In contrast, the second taper (T2) is very gentle and is most obvious in the low basal friction model (LF). After 16.3% bulk shortening T2 reaches about 2–4 degrees in the LF and IF models and is insignificant in the HF model.

We noticed the second taper only because we were using the high-accuracy laser scanner. Looking back through the literature, the same effect can be recognized in wedges shortening over low-friction decollements and layers but was not reported at the time.

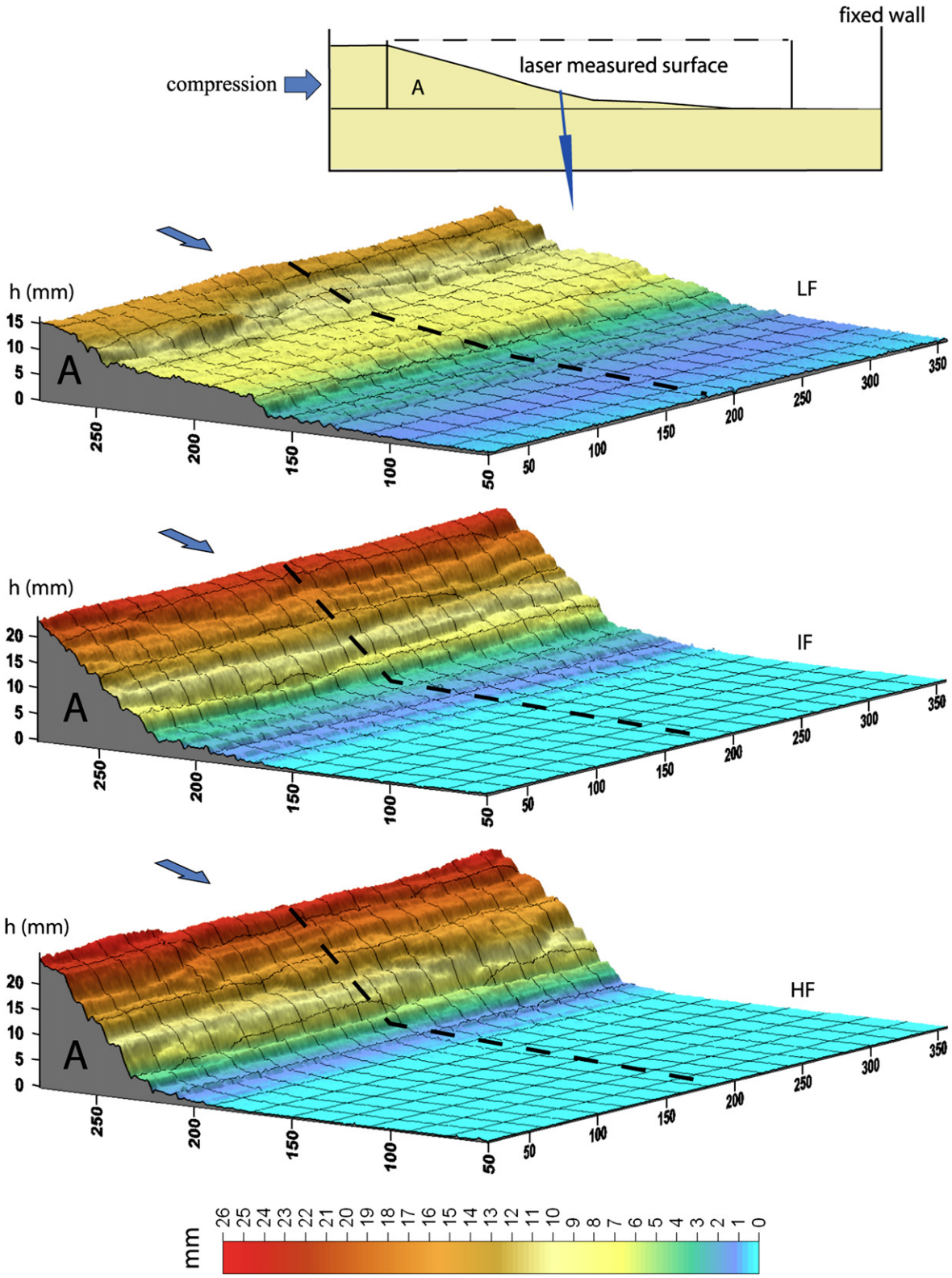

Fig. 3. Shaded relief perspective diagrams of low (LF), intermediate (IF) and high (HF) basal friction models after 16.5% bulk shortening. Measured areas (A) are shown in upper inset. Arrows show shortening direction. The dashed lines along centerline of the models show location of profiles in Fig. 4 (For interpretation of the references to color in this Figure, the reader is referred to the web version of this article).

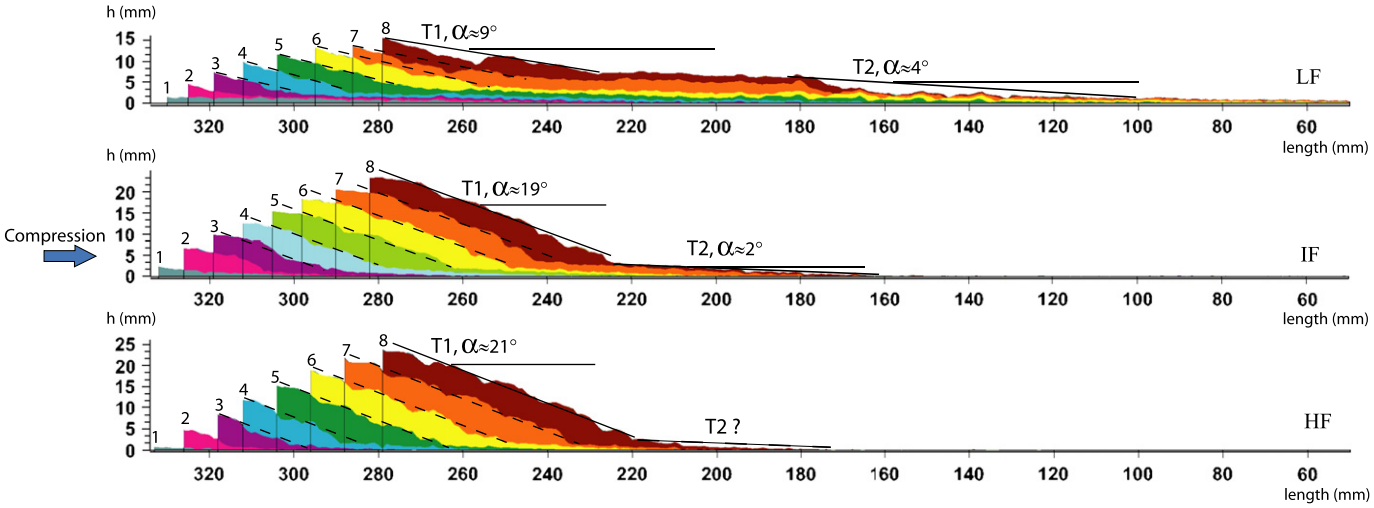

Fig. 4. Sequential topographical profiles along centerlines of three models after 8 × 1 cm increments of horizontal shortening shown by different shading. Wedge height, topographic slopes and localization of deformation are directly correlated with basal friction. The taper surface T1 stays parallel in the IF and HF models after 3 cm bulk shortening and both wedges grow with self-similar geometry. In the LF model T1 changes orientation at different stages and the wedge does not reach to a stable geometry. The two tapers of the wedge (T1 and T2) are most obvious in the LF model (For interpretation of the references to color in this Figure, the reader is referred to the web version of this article).

Within the scanned area, the wedge slopes (T1) remained parallel from the stage of 6% (3 cm) bulk shortening to the final stage (16.3% bulk shortening) in models with higher basal frictions (Fig. 4). This indicates that the wedges in the IF and HF models grow with self similar geometries.

3.3. Surface strain

Surface strains were measured using displacements of selected corners of the passive surface grid by comparing the digital images of initial and final stages (see details in Nilforoushan and Koyi, 2007). Some parts of the grid were overridden by imbricate thrusts and disappeared during deformation. The surviving corners of the initially square cells (12 × 12 mm) on the top and in front of the wedge were used by prepared scripts in MATLAB software to estimate the strain parameters (Fig. 6). Cells within a few centimeters of the side walls were neglected to minimize any direct effect of the side boundaries.

The distortion of each initial square of the grid is illustrated by a calculated strain ellipse (Fig. 6). Such strain ellipses mostly show uniaxial shortening parallel to the shortening direction indicating movements of markers parallel to the shortening direction. As illustrated by the laser measurements (Figs. 3 and 4), displacements of grid intersections on the top surface show that the deformation front advanced further and faster in the model shortened above a low-friction decollement.

We divided all three model surfaces into three zones; wedge top (the zone between rear wall and line AB in Fig. 1), wedge slope and foreland in front of the main wedge, to compare the localization of deformation in different parts of each model (Fig. 7). The longitudinal strain (engineering extension) (Ramsay and Huber, 1983, pp. 281–296) in these zones was estimated by measuring the horizontal length of each zone in the direction of shortening along the middle of

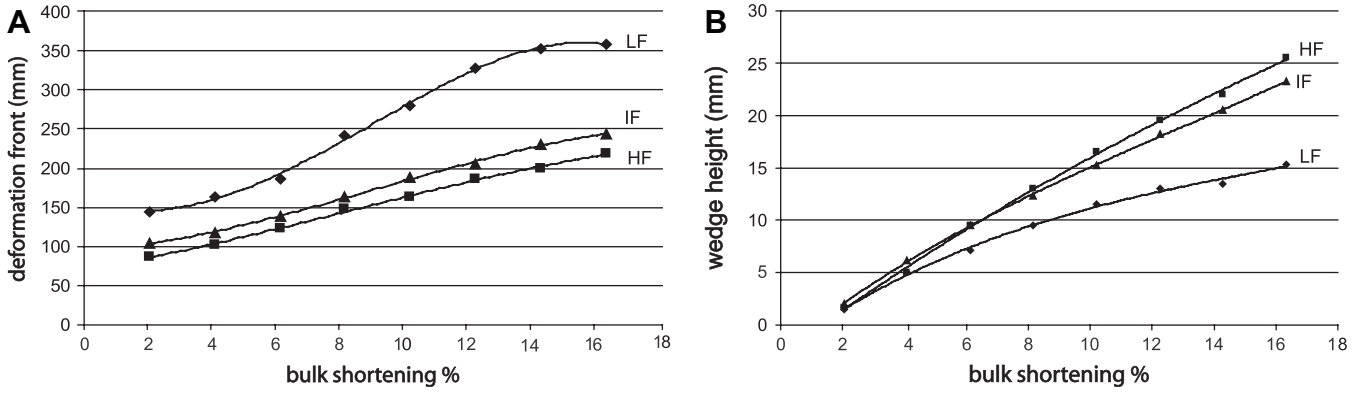

Fig. 5. (A) Progressive migration of deformation front with increasing shortening. (B) Progressive increase in maximum wedge height with increasing shortening. The best fit polynomials show HF and IF models differ significantly from LF model where wedge height is lower and more deformation has advanced. The deformation advances with approximately constant rate in the IF and HF models.

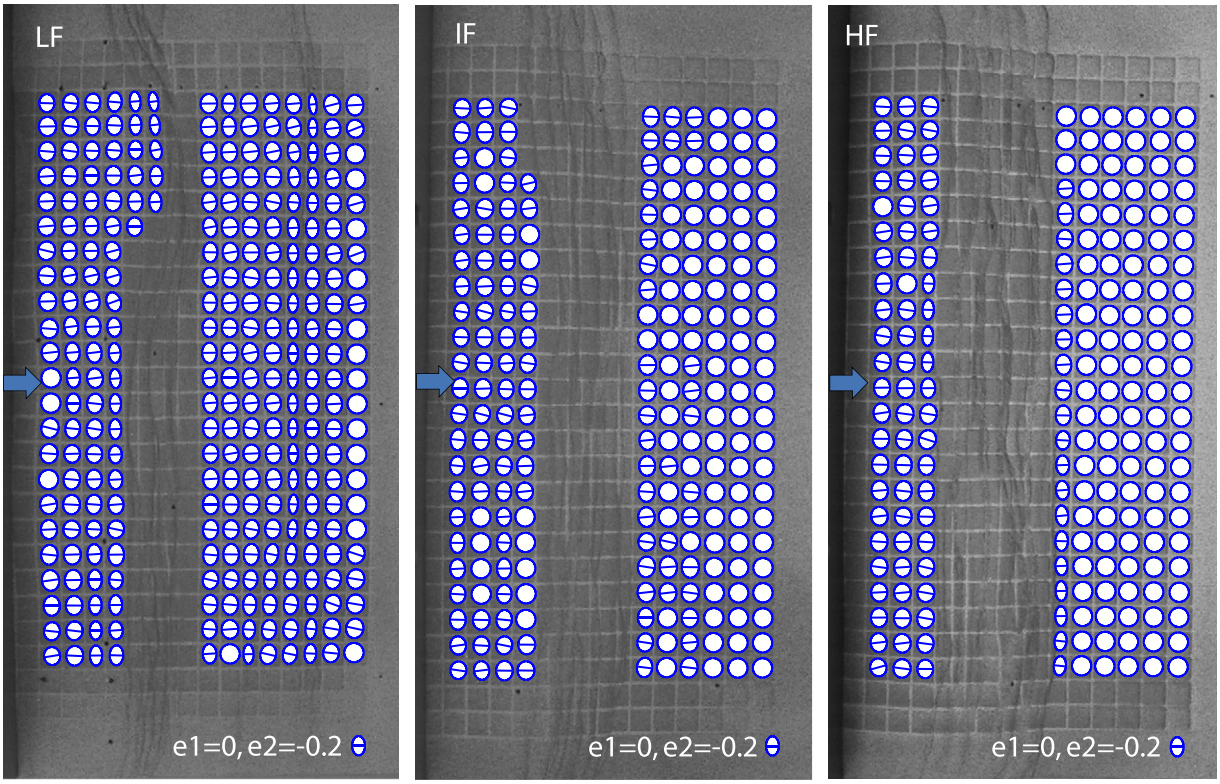

Fig. 6. Finite strain ellipses (of cells with initial dimensions of 12 × 12 mm) superimposed on the cropped images of model surfaces (LF, IF, HF) after 16.3% bulk shortening. Principal strains are scaled by 20, and only e2 principal strain axes are shown for simplicity. Vacant areas indicate lost markers (e.g. overridden by imbricates). Ellipses without axes are the cells with very low strain (|e1| and |e2| are less than 0.05). Arrows show shortening directions.

each model before and after 16.3% bulk shortening. Since the length of these zones differ in the three models, we compute the bulk strain by relating the initial length of the model (490 mm) with its length after 16.3% bulk shortening. In this way, the total bulk shortening (16.3%) is considered to have been 100% and we computed the distribution of this total strain in each of the three zones. Comparison of the results shows that about one-third of the bulk shortening is taken up in the wedge top, whatever the basal friction (Fig. 7). In sharp contrast, the bulk shortening in the main wedge slope (T1) ranges from 40% in LF to 63% in HF (Fig. 7). The foreland takes up more strain (29%) in the LF model and shows only low values in the IF and HF models. The strain associated with the low-friction decollement is diffuse whereas in IF and HF, most of the deformation occurs by thrusting in the wedge slope (zone 2). In general, strain distributions were similar in the IF and HF models (Fig. 7).

To show how deformation developed in the LF model, nine stripes of the model surface parallel to the shortening direction were cropped from the central part of the LF model images (Fig. 8). Together with laser measurements of the scanned area (Fig. 1) these stripes of digital images clearly show the distribution of surface deformation above a low-friction decollement (LF) and illustrate that the basal decollement was active throughout model shortening.

The rate that the deformation front advanced in the LF model was variable. It was low in the initial stages, accelerated in the middle stages and was slower in the final stages. This variable propagation rate might be due to episodic strain distribution (e.g. Mulugeta and Koyi, 1992; Persson, 2001). These observations also indicate that, above a low-friction decollement, the sole thrust does not necessarily obey the stick-slip mode of propagation. Instead, we propose that the sole thrust followed a fast slip-creep mode of advance.

After 8 cm (16.3%) bulk shortening the deformation front was approaching the distal end of the scanned area (Figs. 3, 4 and 8) and shortening of the model was stopped. At this stage two imbricate thrust zones were observed in the LF model surface. It is clear that the deformation front was much further from the location of the frontal thrust that is usually used to interpret the deformation front in natural cases. This suggests that the deformation zone may be wider than generally inferred, particularly above low-friction decollements.

3.4. Volumetric strain

The volumetric strain is the ratio of volume change and initial volume (e.g. Nihei et al., 2000) and is defined as:

$$\varepsilon_v = \frac{V - V0}{V0} \tag{1}$$

where $V0$ is the initial volume of sand in our scanned area and V is the volume after each increment of shortening. In our volume estimations, we assumed uniform deformation above a rigid basement and the same displacements for the materials

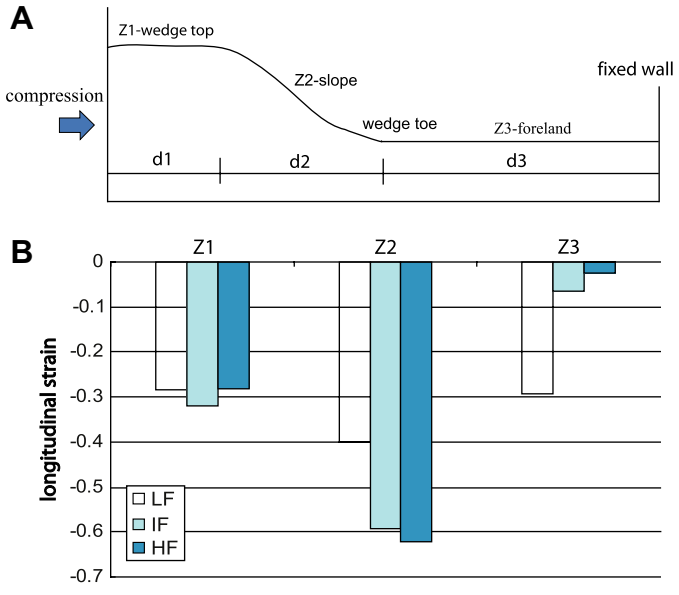

Fig. 7. (A) Schematic side view of models that distinguishes three zones of deformation, wedge top Z1, wedge slope Z2 and foreland Z3. Z1 is defined as the zone between the moving wall and the scanned area, Z2 is from edge of the wedge top to the wedge toe, and the foreland is Z3. The d1, d2 and d3 are horizontal lengths of these zones measured before and after shortening (16.3% bulk shortening). (B) Illustration of longitudinal (engineering) strain distribution in three different models at 16.3% bulk shortening. A high amount of strain occurred in the wedge slope zone where imbrication and thrusting take up most of shortening. The LF model includes the second imbricate zone and therefore undergoes more shortening in Z3.

in deep layers beneath the control points as on the surface. As earlier studies have shown that layer parallel shortening increases with depth in sand models (e.g. Koyi, 1995), our volume estimations are thus only approximate minima.

To estimate the overall volume changes in the sandpack beneath the scanned area, we took into account the forward transfer of material from the rear zone (between the moving wall and the scanned area, Fig. 1). However, we calculated the volumetric strain for $2.5 \times 33.8 \times 28.5$ cm ≈ 2400 cm^3 of sand after each 1 cm increment of shortening. All three models showed volumetric strain less than 1% after 1 cm bulk shortening (Fig. 10). In LF, the volumetric-strain decreased slowly to $-5 \pm 0.5\%$ by 12% bulk shortening and then did not change significantly after further shortening (Fig. 10). In contrast, the higher basal frictions in the IF and HF models built the sandpack to steeper tapers and involved greater lateral and vertical compaction. By the final stage of shortening (after 8 cm or 16.3% bulk shortening) the estimated volumetric-strains were $-5 \pm 0.5\%$, $-9.5 \pm 0.5\%$ and $-12.5 \pm 0.5\%$ for the LF, IF and HF models, respectively, illustrating a direct correlation between volume reduction and basal friction (Fig. 10 and Table 1).

4. Discussion

4.1. Model tapers

The critical taper wedge theory (e.g. Davis et al., 1983; Dahlen, 1990) states that fold-thrust belts or accretionary wedges are mechanically analogous to a wedge of sand pushed in front of the blade of a moving bulldozer. The height and width of the wedge increase to reach a steady or critical geometry. The surface slope (α) of the critical wedge and its basal dip (β) form the so-called critical taper, $\alpha + \beta$which mainly depends on basal and internal friction of the deformed units ($\mu_b$and μ respectively). The critical taper for dry sand in cohesionless wedges can be approximated (e.g. Davis et al., 1983; Mulugeta, 1988; Dahlen, 1990) by:

$$\alpha + \beta \cong \left(\frac{1 - \sin\theta}{1 + \sin\theta}\right)(\beta + \mu_b) \qquad (2)$$

where μ_b is the basal friction and θ is the angle of internal friction of the deformed units. According to Davis et al. (1983); Mulugeta (1988) and Dahlen (1990), this equation is applicable when $\mu_b \ll \mu$ where $\mu = 0.57$ is the coefficient of internal friction. The sand used in our models is not entirely cohesionless, it has a small amount of cohesion ($C = \sim 140$ Pa). However, we considered this cohesion to be small and apply the above equation (eq. 2) to estimate the taper in our models. Substituting $\beta = 0$ (horizontal rigid basement), $\theta = 30^\circ$ (for dry sand used in our models) and $\mu_b = 0.36$, 0.5 and 0.7 results in $\alpha = 7^\circ$, 9.7° and 13.5° for the LF, IF and HF models, respectively. The measured model tapers for T1 (the main wedge), $9 \pm 1^\circ$, $19 \pm 1^\circ$ and $21 \pm 1^\circ$ after 16.3% bulk shortening in the LF, IF and HF models respectively, differ from theoretical predictions. The constant α of T1 in the IF and HF models after 3 cm bulk shortening implies that these wedges were critical after that stage (Figs. 4 and 9). In contrast α was still changing in the LF model even after 16.3% bulk shortening, suggesting that it did not reach a critical taper. The discrepancies in the simplified equation (2) increase significantly in the IF and HF models, where the basal friction coefficients, $\mu_b = 0.5$ and $\mu_b = 0.7$ respectively, approach or are greater than the internal friction coefficient of the sand ($\mu = 0.57$) (Mulugeta, 1988; Dahlen, 1990). Therefore using eq. (2) is not a good approximation for critical taper approximations when $\mu_b >> \mu$. However, since the basal friction coefficient (0.37) in the LF model is smaller than the internal friction of sand (0.57), the difference between the measured (T1) and theoretical critical tapers (7° vs. $9 \pm 1^\circ$) is not significant and suggests that LF taper is possibly close to reach the critical taper in later stages. Since the low-friction decollement is not a ductile layer in our model, we can not attribute the discrepancy between the theoretical and measured tapers to deformation of the decollement itself, as has been suggested by Ford (2004). In addition to using a simplified equation (eq. 2), the sand used in the models had some cohesion which may slightly contribute to these discrepancies. Our model results suggest that eq. (2) fits best to low-friction rigid decollements (like aluminum sheet in our experiment). This relatively good fit (± 2 degrees) could be due the low degree of sand compaction (i.e. less change in the mechanical behavior of the modeling material) seen in the LF models. This is in line with the conclusions of Mulugeta (1988) and Lohrmann et al. (2003) where they argued that discrepancies between

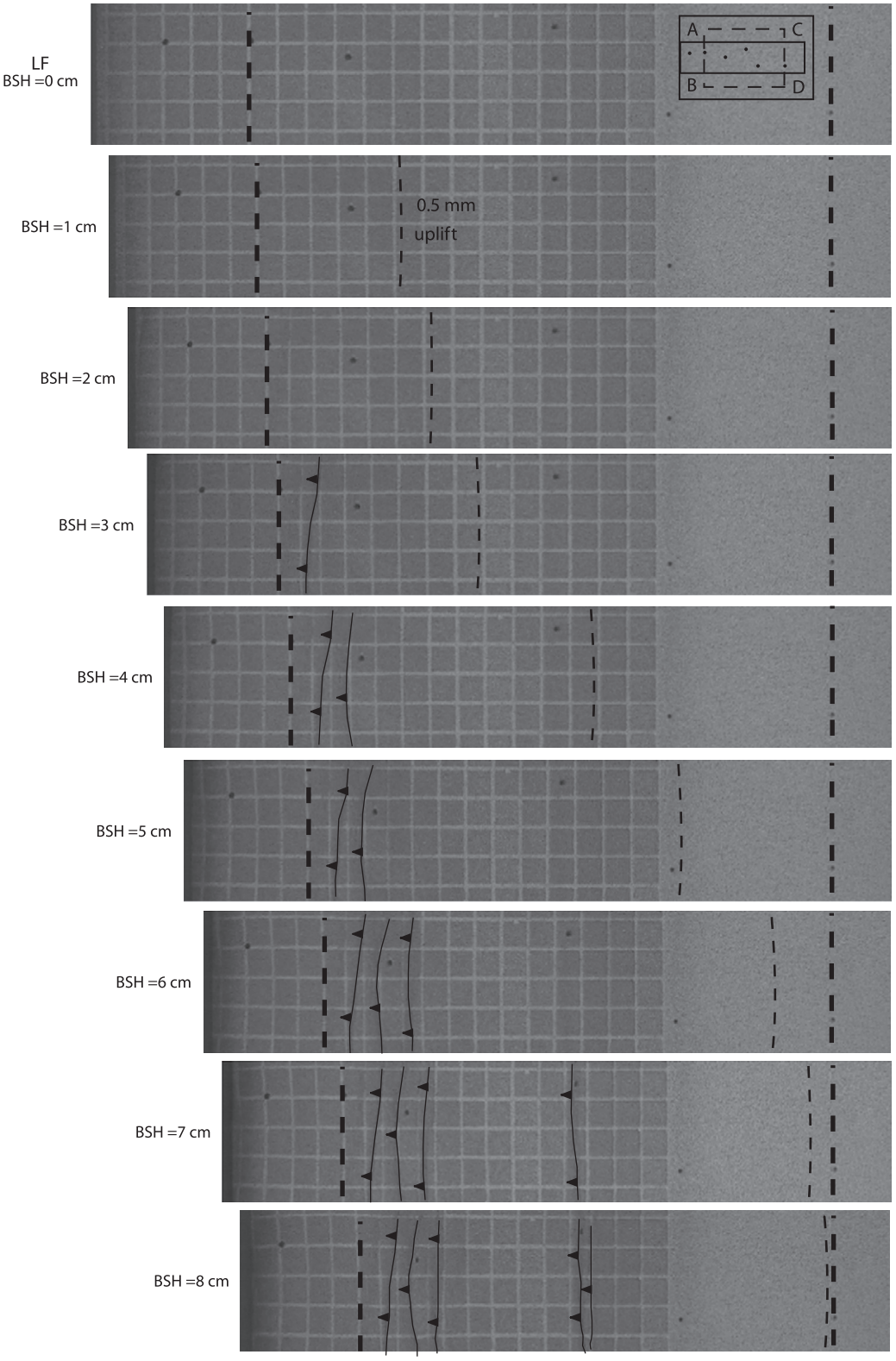

Fig. 8. Central image stripes of the LF model surface with line drawings of thrust faults emerging on the surface before and after 8 stages of bulk shortening. Location of these stripes is outlined in the first stripe. Thick dashed lines show part of laser scanned area. The thin dashed line shows the deformation front (where the model surface rises 0.5 mm) and shows the progress of deformation and decollement activity.

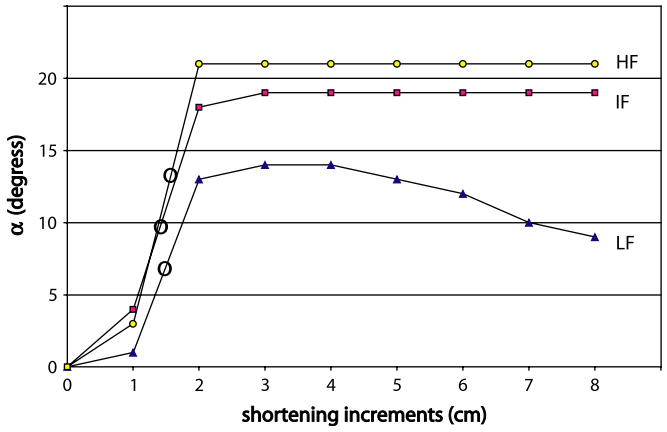

Fig. 9. Variation of α with shortening in the three models (IF, LF and HF) extracted from Fig. 4. The HF and IF models reach a critical stage and α does not change any more, while LF does not become critical until 16.5% bulk shortening. The big circles on the graphs show theoretical values α which are different from our measured values, especially in the IF and HF models.

theoretical and experimental wedge tapers could be due to change in material properties during accretion whereas the theoretical taper equation assumes that the density and the various Coulomb parameters remain constant during accretion. In our IF and HF models, the modeling material undergoes a higher amount of volume loss (ca. 10% and 13%) and thus change its mechanical behavior during the deformation.

The difference between a low-friction rigid decollement and a deformable viscous decollement (which is usually used in many analogue experiments to simulate salt or shale, e.g. Davis and Engelder, 1985; Koyi, 1988; Cotton and Koyi, 2000; Schreurs et al., 2001) is very important when discussing the taper angle and relating wedge shape to basal friction. However, these two types of decollements can have mechanically similar effect in that they provide low resistance against movement of the overlying sediments. However, deformation of a viscous decollement (by e.g. thickness change or diapirism) can change the geometry of the wedge and thereby the taper. In our models which focused on quantifying the effect of basal friction on volumetric change, we used a rigid decollement in the low-friction models.

It is worth mentioning that, approximating the entire surface slope including inner and outer wedges, with a single taper (as is usual) implies a taper 4° smaller than that measured for T1 in the LF model. However, assuming inner and outer wedges, as reported here, may change the implications connecting the deformation mechanisms involved in fold-thrust belts and accretionary prisms with low-friction decollement.

4.2. Volumetric-strain

Many previous workers have emphasized the effect of basal friction on the kinematics and geometry of accretionary wedges and fold-thrust belts (e.g. Davis et al., 1983; Dahlen et al., 1984; Davis and Engelder, 1985; Mulugeta, 1988; Cotton and Koyi, 2000; Bahroudi and Koyi, 2003; Ford, 2004; Koyi and Cotton, 2004; Bonini, 2007). Here we add that basal friction directly influences the degree and distribution of volumetric strain (Fig. 10 and Table 1). The volume reduction estimated in our models is due to lateral compaction of the sand layers as the sand grains are repacked during the shortening, frictional slip along sand grain contacts (Nihei et al., 2000) and gravitational compaction with the increase in thickness (Koyi et al., 2004; Koyi and Maillot, 2007). Since the individual sand grains can not deform internally under model conditions, this volume decrease is taken up by a reduction in the bulk porosity of the sand layer (Koyi and Vendeville, 2003; Koyi et al., 2004). In nature, such volumetric-strains result in porosity reduction in deformed lithologies and will have a negative impact on potential reservoir quality.

If we divide the volume of the sand, estimated after a succession of shortening increments, by the lateral extent of the scanned area (AB = 338 mm, Fig. 1B) and then by the thickness of the models (25 mm), we end up with the restored length of the models after each increment. The incremental length changes (the difference between the initial and restored

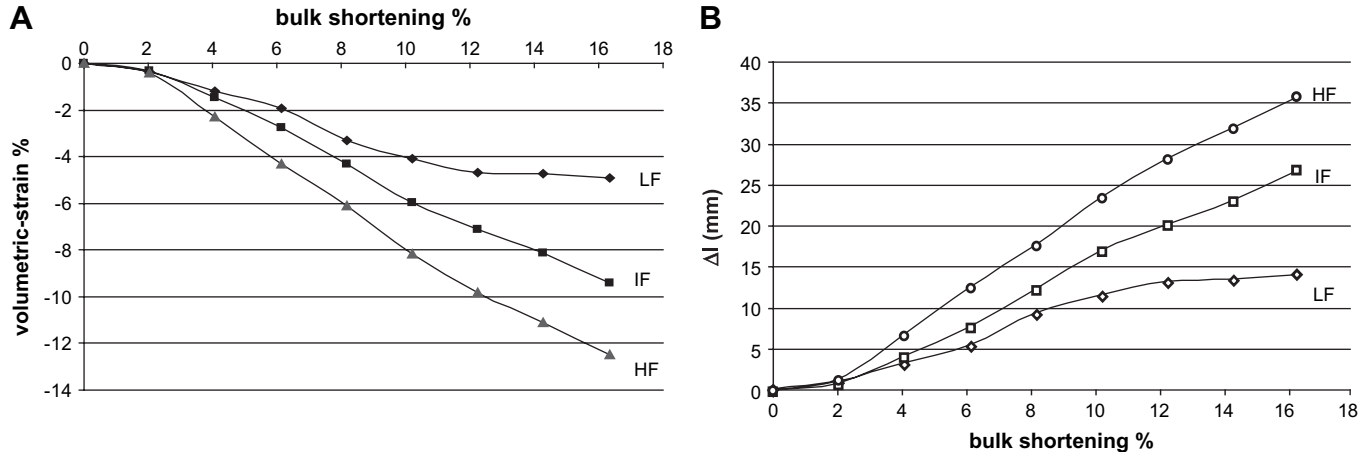

Fig. 10. (A) Progressive volumetric-strain for 3 models, measured after each increment of 1 cm shortening. A high correlation between volume loss and basal friction is observed. (B) Length change (the difference between initial length of study area (285 mm) and restored length deduced from volumetric-strains) vs. bulk shortening.

Table 1
Comparison of the low (LF), intermediate (IF) and high (HF) basal friction models at the last stage (16.3%) of bulk shortening

Parameter	Basal friction coefficient	Max. height of the wedge (mm)	Deformation front advance (mm)	T1 taper (degrees)	Volumetric strain (%)
LF	0.36	26	358	9	−5
IF	0.50	24	244	19	−9.5
HF	0.70	15	228	21	−12.5

The deformation front was measured from initial position of rear wall. The heights, deformation fronts and tapers were extracted from central profiles (as indicated in Fig. 4).

lengths of the scanned area parallel to the shortening direction) follow the same trend of volumetric strains (Fig. 10A and B). These two graphs look similar since the volumes have been down-scaled by the constant area. Our measurements show that bedding-parallel shortening is greater above high-friction decollements than above low-friction decollements. This suggests that restored sections of areas shortened above a high-friction decollement do not correctly reproduce the total amount of shortening if bed-length shortening (i.e. penetrative strain) is not taken into account in the restoration (see for example Cooper et al., 1983).

Layer parallel shortening (LPS), along with folding and imbrication, is an important component of deformation in fold-thrust belts (e.g. Dahlstrom, 1969; Cooper, 1983; Marshak and Woodward, 1988; Mitra, 1994; Koyi, 1995; Skourlis and Doutsos, 2003; Koyi et al., 2004). Our models show that basal friction strongly influences the amount of LPS in the shortened layers. Koyi et al. (2004) showed that the amount of LPS generally increases from shallow layers to deeper layers in sand models and depends on basal friction. Here too, our measurements of the surface of three models show the dependency of LPS and basal friction. By measuring the incremental and total surface penetrative strain above a frictional and a viscous layer decollement, Nilforoushan and Koyi (2007) also showed that the area-loss above an intermediate-friction decollement was greater than that above a viscous decollement.

Davis and Engelder (1985) argued that the amount of LPS beyond the frontal folds in the Appalachian Plateau is about 10–20% and it depends on the distribution of the basal salt, i.e. a weak decollement. Other workers have also estimated 9–14% LPS in the southern Appalachians (Whitaker and Bartholomew 1999) and 20% LPS in the Pyrenees (Koyi et al., 2004). Therefore this component of shortening and its correlation with basal friction should be taken into account when restoring geological sections.

4.3. Role of basal friction in the Zagros fold-thrust belt

Recent GPS studies of the Zagros fold-thrust belt indicate that it is currently shortening at about 10 mm/yr in SE Zagros and about 5 mm/yr in NW Zagros (Nilforoushan et al., 2003; Vernant et al., 2004; Hessami et al., 2006; Walpersdorf et al., 2006). The relatively dense GPS networks in the Zagros (Hessami et al., 2006; Walpersdorf et al., 2006) show that deformation resulting from this shortening is not distributed uniformly and differs from the NW to the SE Zagros partly due to presence of a salt layer underlying the SE Zagros. The salt layer beneath the Zagros fold-thrust belt have been considered as an example of a natural low-friction decollement (e.g. Falcon, 1969; Kent, 1979; Davis and Engelder, 1985; Talbot and Alavi, 1996; Bahroudi and Koyi, 2003). Our low-friction rigid plate which provides a low-friction decollement can be compared with the low-friction decollement provided by the Hormuz salt in the Zagros fold-thrust belt. Similarly, the high-friction decollement models can be compared to those areas of the Zagros fold-thrust belt where this weak decollement (i.e. Hormuz salt) is missing or is very thin. The NW Zagros has no basal salt and exemplifies a high-friction decollement. Decollements with low coefficients of friction allow deformation in the overlying material to propagate and spread towards the foreland faster than decollements with higher coefficients of friction (Dahlen et al., 1984; Cotton and Koyi, 2000; Costa and Vendeville, 2002; Ford, 2004; Koyi and Cotton, 2004). By contrast, the material above basal decollements with high friction slide and spread more slowly so that they thicken and compact to higher wedges with steeper slopes like the NW Zagros (Fig. 11). The low and high topographies in the SE and NW Zagros, respectively partly reflect the presence or lack of the salt decollement (i.e. low- or high-friction decollement, respectively).

To approximate the Zagros slopes, we used DEM data (1 km digital elevation model GLOBE, available at http://www.ngdc.noaa.gov/mgg/topo/globe.html), extracted the elevations along the selected profiles and fit a straight line to those elevations to define the slopes. For profiles 1–3 (Fig. 11), there are some points on the wedge top like our models which we did not use: we only fit a straight line connecting the points on the slope.

Topographical profiles across the two wedges in the NW and the SE Zagros show very gentle topographical slopes that differ in α. The mean slopes decrease from $\alpha = 1.06^\circ$ (profiles 1–3) in NW Zagros to $\alpha = 0.35^\circ$ in SE Zagros (profiles 4–6). If we assume a basal dip of $\beta = 2^\circ$ and $\beta = 0.5^\circ$ for the NW and the SE Zagros respectively (e.g. Davis and Engelder, 1985; McQuarrie, 2004) then $\alpha + \beta \approx 3^\circ$ and $\alpha + \beta \approx 0.85^\circ$ for these two wedges respectively. These differences partly relate to friction along the decollement which influences the topographies and tapers. However, model results suggest that in the NW Zagros, where a weak decollement is missing, cover sediments undergo higher lateral compaction and more LPS is expected relative to the SE Zagros where a layer of Hormuz salt acts as a weak decollement.

In addition to friction along the decollement, other factors that influence the taper are: the presence of basement faults

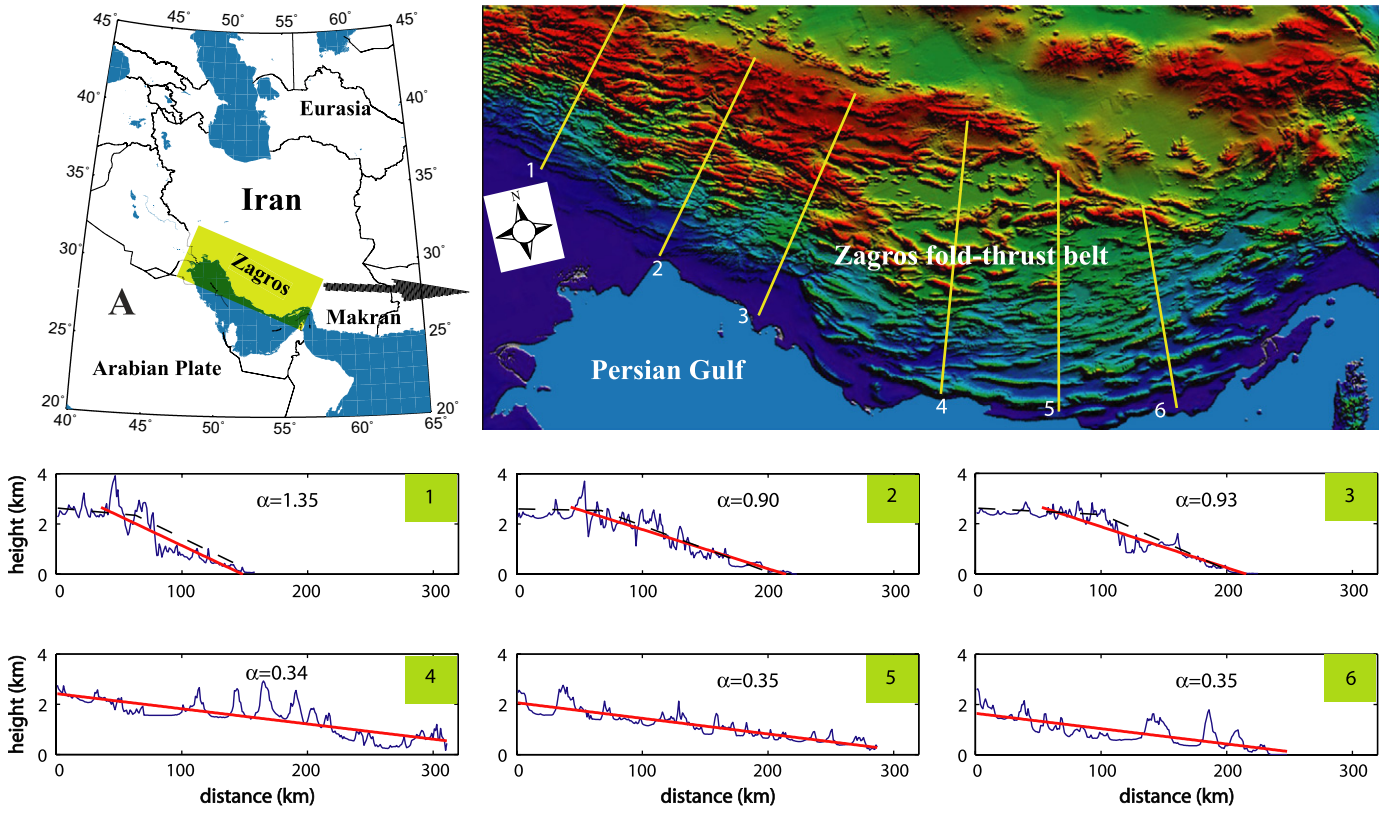

Fig. 11. (A) Map of Iran with the study area shaded. (B) Shaded relief of 1 km digital elevation model (GLOBE, http://www.ngdc.noaa.gov/mgg/topo/globe.html) with six topographic profiles (nos. 1–6) perpendicular to the main structural trends across Zagros. In NW Zagros (profiles 1–3), where high friction is dominant (i.e. absence of Hormuz Salt) high elevations and relatively steep tapers are observed. In SE Zagros (profiles 4–6), where Hormuz Salt acts as a low-friction decollement, a wide zone of deformation (more than 300 km across the belt) with lower taper is observed. Dashed lines in profiles 1–3 approximate the wedge geometry (For interpretation of the references to color in this Figure, the reader is referred to the web version of this article).

(e.g. Jackson, 1980; Ni and Barazangi, 1986; Berberian, 1995; Hessami et al., 2001; McQuarrie, 2004; Mouthereau et al., 2006), erosion and sedimentation (Huene and Ranero, 2003), pore fluid pressure and its influence on the mechanical properties of the deformed wedge (Kukowski and Schillhorn, 1996), foreland flexure and the convergent rate (Simpson, 2006). None of the above parameters are included in our models.

5. Conclusion

This study used a high-accuracy laser scanner to show systematically the influence of basal friction on surface and volumetric strain in models of fold-thrust belts and accretionary prisms. Our results indicate that, in addition to influencing the kinematics and geometry of the wedge, there are direct correlations between volume reductions and basal friction; increasing basal friction increases volume reduction. Applied to nature, our model results indicate that compaction and penetrative strain are expected to be greater in fold-thrust belts shortened above high-friction decollements than in fold-thrust belts shortened above low-friction decollements.

Model results also show that surface strain is increasingly localized as friction along the basal decollement increases. Accurate vertical measurements show that the deformation front is much farther forward than the frontal thrusts usually considered as the deformation front, especially in our LF models.

Our sub-millimetric (±0.1 mm) height measurements reveal that our experimental wedges developed and maintained inner and outer tapers throughout their shortening, particularly in the LF model.

Profiles across the Zagros fold-thrust-belt in Iran suggest similar dependencies of topography and taper on basal friction as profiles along our models.

Acknowledgments

We would like to thank the reviewers Mary Ford and Ken McCaffrey for thorough and constructive reviews and the Editor Robert E. Holdsworth for handling the manuscript. F.N. acknowledges a PhD grant from the Uppsala University. H.A.K. is funded by the Swedish Research Council (VR).

References

Agarwal, K.K., Agrawal, G.K., 2002. Analogue sandbox models of thrust wedges with variable basal frictions. Gondwana Research 5, 641–647.

Bahroudi, A., Koyi, H.A., 2003. The effect of spatial distribution of Hormuz salt on deformation style in the Zagros fold and thrust belt: an analogue modeling approach. Journal of the Geological Society, London 160, 719–733.

Berberian, M., 1995. Master "blind" thrust faults hidden under the Zagros folds; active basement tectonics and surface morphotectonics. Tectonophysics 241, 193–224.

Bonini, M., 2001. Passive roof thrusting and forelandward fold propagation in scale brittle-ductile physical models of thrust wedges. Journal of Geophysical Research 106, 2291–2311.

Bonini, M., 2007. Deformation patterns and structural vergence in brittle-ductile thrust wedges: An additional analogue modelling perspective. Journal of Structural Geology 29, 141–158.

Buiter, S.J.H., Schreurs, G. (Eds.), 2006. Analogue and Numerical Modeling of crustal-scale processes. Geological Society London, Special publications, p. 253.

Calassou, S., Larroque, C., Malavieille, J., 1993. Transfer zones of deformation in thrust wedges: an experimental study. Tectonophysics 221, 325–344.

Colletta, B., Letouzey, J., Pinedo, R., Ballard, J.F., Bale, P., 1991. Computerized X-ray tomography analysis of sandbox models; examples of thin-skinned thrust systems. Geology 19, 1063–1067.

Cooper, M.A., 1983. The calculation of bulk strain in oblique and inclined balanced sections: Journal of Structural Geology 5, 161–165.

Cooper, M.A., Garton, M.R., Hossack, J.R., 1983. The origin of the Basse Normandie Duplex, Boulonnais, France. Journal of Structural Geology 5, 139–152.

Costa, E., Vendeville, B.B., 2002. Experimental insights on the geometry and kinematics of fold-and-thrust belt above weak, viscous evaporatic decollement. Journal of Structural Geology 24, 1729–1739.

Cotton, J.T., Koyi, H.A., 2000. Modeling of thrust fronts above ductile and frictional decollements: application to structures in the salt range and Potwar plateau, Pakistan. Geological Society of America Bulletin 112, 351–363.

Dahlen, F.A., 1990. Critical taper model of fold-thrust belts and accretionary wedges. Annual Review of Earth and Planetary Sciences 18, 55–99.

Dahlen, F.A., Suppe, J., Davis, D., 1984. Mechanics of fold-and-thrust belts and accretionary wedges; cohesive Coulomb theory. Journal of Geophysical Research 89, 10087–10101.

Dahlstrom, C.D.A., 1969. Balanced cross sections. Canadian Journal of Earth Sciences 6, 743–747.

Davis, D.M., Engelder, T., 1985. The role of salt in fold-and-thrust belts. Tectonophysics 119, 67–88.

Davis, D.M., Suppe, J., Dahlen, F.A., 1983. Mechanics of fold-and-thrust belts and accretionary wedges. Journal of Geophysical Research 88, 1153–1172.

Davy, P., Cobbold, P.R., 1991. Experimental and Numerical Modeling of Continental Deformation. Tectonophysics. In: Cobbold, P.R. (Ed.), Experiments on shortening of 4-layer model of continental lithosphere, 188, pp. 1–25.

Falcon, N.L., 1969. Problems of the relationship between surface structure and deep displacements illustrated by the Zagros range. In: Kent, P.E. (Ed.), Time and Place in Orogeny. Geological Society Special Publications 3, London, pp. 9–22.

Ford, M., 2004. Depositional wedge tops: interaction between low basal friction external orogenic wedges and flexural foreland basins. Basin Research 16 (3), 361–375, doi:10.1111/j.1365-2117.2004.00236.x.

Gutscher, M.A., Kukowski, N., Malavieille, J., Lallemand, S., 1996. Cyclical behavior of thrust wedges; insights from high basal friction sandbox experiments. Geology 24, 135–138.

Gutscher, M.A., Kukowski, N., Malavieille, J., Lallemand, S., 1998. Material transfer in accretionary wedges from analysis of a systematic series of analog experiments. Journal of Structural Geology 20, 407–416.

Hessami, K., Koyi, H., Talbot, C.J., 2001. The Significance of Strike-slip faulting in the basement of the Zagros fold and thrust belt. Journal of Petroleum Geology 24, 5–28.

Hessami, K., Nilforoushan, F., Talbot, C.J., 2006. Active deformation within the Zagros Mountains deduced from GPS measurements. Journal of the Geological Society London 163, 143–148.

Huene, R. Von, Ranero, C.R., 2003. Subduction erosion and basal friction along the sediment-starved convergent margin off Antofagasta, Chile, Journal of Geophysical Research 108 (B2), 2079, doi:10.1029/2001JB001569.

Huiqui, L., McClay, K.R., Powell, D., 1992. Physical models of thrust wedges. In: McClay, K.R. (Ed.), Thrust Tectonics. Chapman and Hall, London, UK, pp. 71–81.

Jackson, J.A., 1980. Reactivation of basement faults and crustal shortening in orogenic belts. Nature 283, 343–346.

Kent, P.E., 1979. The emergent Hormuz salt plugs of southern Iran. Journal of Petroleum Geology 2, 117–144.

Koyi, H.A., 1988. Experimental modeling of the role of gravity and lateral shortening in the Zagros mountain belt. AAPG Bulletin 72, 381–1394.

Koyi, H., 1995. Mode of internal deformation in sand wedges. Journal of Structural Geology 17, 293–300.

Koyi, H.A., 1997. Analogue modeling; from a qualitative to a quantitative technique; a historical outline. Journal of Petroleum Geology 20, 223–238.

Koyi, H.A., Cotton, J., 2004. Experimental insights on the geometry and kinematics of fold-and-thrust belts above weak, viscous evaporitic decollement; a discussion. Journal of Structural Geology 26, 2139–2141.

Koyi, H.A., Maillot, B., 2007. Quantifying the effect of ramp dip and friction on thickness change of hanging wall units. Journal of Structural Geology 29, 924–932.

Koyi, H.A., Petersen, K., 1993. The influence of basement faults on the development of salt structures in the Danish Basin. Marine and Petroleum Geology 10, 82–94.

Koyi, H.A., Vendeville, B., 2003. The effect of decollement dip on geometry and kinematics of model accretionary wedges Journal of Structural Geology 25, 1445–1450.

Koyi, H., Hessami, K., Teixell, A., 2000. Epicenter distribution and magnitude of earthquakes in fold-thrust belts: insights from sandbox modelling. Geophysical Research Letters 27, 273–276.

Koyi, H.A., Sans, M., Teixell, A., Cotton, J., Zeyen, H., 2004. The significance of penetrative strain in the restoration of shortened layers—Insights from sand models and the Spanish Pyrenees. In: McClay, K.R. (Ed.), Thrust Tectonics and Hydrocarbon Systems, 82. AAPG Memoir, pp. 1–16.

Kukowski, N., Schillhorn, T., 1996. Modeling of fully coupled transient fluid and heat transport in growing accretionary wedges. EOS 77 (46), 701.

Lallemand, S.E., Schnuerle, P., Malavieille, J., 1994. Coulomb theory applied to accretionary and nonaccretionary wedges; possible causes for tectonic erosion and/or frontal accretion. Journal of Geophysical Research 99, 12033–12055.

Liu, H., McClay, K.R., Powell, D., 1992. Physical models of thrust wedge. In: McClay, K.R. (Ed.), Thrust Tectonics. Chapman and Hall, London, pp. 71–81.

Lohrmann, J., Kukowski, N., Adam, J., Oncken, O., 2003. The impact of analogue material parameters on the geometry, kinematics, and dynamics of convergent sand wedges. Journal of Structural Geology 25, 1691–1711.

Maillot, B., Koyi, H., 2006. Thrust dip and thrust refraction in fault-bend-folds: analogue models and theoretical predictions. Journal of Structural Geology 28, 36–49.

Malavieille, J., 1984. Modelisation experimentale des chevauchements imbriques: application aux chaines des montagnes. Bulletin de la Societe Geologique de France 26, 129–138.

Marshak, S., Woodward, N.B., 1988. Introduction to cross section balancing, in basicmethods. In: Marshak, S., Mitra, G. (Eds.), Structural Geology. Prentice Hall, Englewood Cliffs, NJ, pp. 303–332.

McQuarrie, N., 2004. Crustal scale geometry of the Zagros fold-thrust belt, Iran. Journal of Structural Geology 26, 519–535.

Mitra, G., 1994. Strain variation in thrust sheets across the Sevier fold-and-thrust belt (Idaho-Utah-Wyoming): implications for section restoration and wedge taper evolution. Journal of Structral Geology 6, 51–61.

Mourgues, R., Cobbold, P.R., 2006. Thrust wedges and fluid overpressures: Sandbox models involving pore fluids, Journal of Geophysical Research 111, B05404, doi:10.1029/2004JB003441.

Mouthereau, F., Lacombe, O., Meyer, B., 2006. The Zagros folded belt (Fars, Iran): constraints from topography and critical wedge modeling. Geophysical Journal International 165, 336–356, doi:10.1111/j.1365-246X.2006.02855.x.

Mulugeta, G., 1988. Modeling the geometry of Coulomb thrust wedges. Journal of Structural Geology 10, 847–859.

Mulugeta, G., Koyi, H., 1987. Three-dimensional geometry and kinematics of experimental piggyback thrusting. Geology 15, 1052–1056.

Mulugeta, G., Koyi, H., 1992. Episodic accretion and strain partitioning in a model sand wedge. Tectonophysics 202, 319–333.

Ni, J., Barazangi, M., 1986. Seismotectonics of the Zagros continental collision zone and a comparison with the Himalayas. Journal of Geophysical Research 91, 8205–8218.

Nihei, K.T., Hilbert Jr., L.B., Cook, N.G.W., Nakagawa, S., Myer, L.R., 2000. Frictional effects on the volumetric strain of sandstone. International Journal of Rock Mechanics and Mining Sciences 37, 121–132.

Nieuwland, D.A., Leutscher, J.H., Gast, J., 2000. Wedge equilibrium in fold-and-thrust belts: prediction of out-of-sequence thrusting based on sandbox experiments and natural examples. Geologie en Mijnbouw, Netherlands Journal of Geosciences 79, 81–91.

Nilforoushan, F., Koyi, A.H., 2007. Displacement fields and finite strains in a sandbox model simulating a fold-thrust-belt, Geophysical Journal International 169, 1341–1355, doi:10.1111/j.1365-246X.2007.03341.x.

Nilforoushan, F., Masson, F., Vernant, P., Vigny, C., Martinod, J., Abbassi, M., Nankali, H., Hatzfeld, D., Bayer, R., Tavakoli, F., Ashtiani, A., Doerflinger, E., Daignières, M., Collard, P., Chéry, J., 2003. GPS network monitors the Arabia-Eurasia collision deformation in Iran. Journal of Geodesy 77, 411–422.

Persson, K., 2001. In: Koyi, H.A., Mancktelow, N. (Eds.), Analogue and Numerical Modelling of Tectonics Geological Society of America, Memoir. Effective indenters and the development of double-vergent orogens: insight from analogue sand models, 193, pp. 191–206.

Ramsay, J., Huber, M., 1983. The Techniques of Modern Structural Geology. Volume 1: Strain Analysis. Academic Press, San Diego, 307 pp.

Schott, B., Koyi, H.A., 2001. Estimating basal friction in accretionary wedges from the geometry and spacing of frontal faults, Earth and Planetary Science Letters 194, 221–227.

Schreurs, G., Buiter, S.J.H., Boutelier, D., Corti, G., Costa, E., Cruden, A.R., Daniel, J.M., Hoth, S., Koyi, H.A., Kukowski, N., Lohrmann, J., Ravaglia, A., Schlische, R.W., Withjack, M.O., Yamada, Y., Cavozzi, C., Delventisette, C., Elder Brady, J.A., Hoffmann-Rothe, A., Mengus, J.M., Montanari, D., Nilforoushan, F., 2006. In: Buiter, S.J.H., Schreurs, G. (Eds.), Analogue and Numerical Modelling of Crustal-Scale Processes. Analogue benchmarks of shortening and extension experiments, 253. Geological Society, London, Special Publications, pp. 1–27.

Schreurs, G., Hänni, R., Vock, P., 2001. In: KoyiH.A., Mancktelow, N.D. (Eds.), Tectonic Modeling: A Volume in Honor of Hans Ramberg. Geological Society of America Memoir. Four-dimensional analysis of analog models: Experiments on transfer zones in fold and thrust belts, 193, pp. 179–190.

Simpson, G.D.H., 2006. Modeling interactions between fold-thrust belt deformation, foreland flexure and surface mass transport. Basin Research 18, 125–143, doi:10.1111/j.1365-2117.2006.00287.x.

Skourlis, K., Doutsos, T., 2003. The Pindos Fold-and-thrust belt (Greece): inversion kinematics of a passive continental margin. International Journal of Earth Sciences 92, 891–903, doi:10.1007/s00531-003-0365-4.

Swantesson, J.O.H., 2005. Weathering and erosion of rock carvings in Sweden during the period 1994-2003. In: Micro Mapping with Laser Scanner for Assessment of Breakdown Rates, 29. Karlstad University Studies, p. 99.

Swantesson, J.O.H., Gustavson, H., 2005. Interpretation of ancient runic inscriptions by laser scanning. In: Bowman, A.K., Brady, M. (Eds.), Images and Artefacts of the Ancient World. Oxford University Press, pp. 35–43.

Swantesson, J.O.H., Moses, C.A., Berg, G.E., Jansson, M.J., 2006. Methods for measuring shore platform micro erosion: A comparison of the micro-erosion meter and laser scanner. Zeitschrift für Geomorphologie N.F. Vol. 144 (Suppl.), 1–17.

Talbot, C.J., Alavi, M., 1996. The past of a future syntaxis across the Zagros. In: Alsop, G.I., Blundell, D.J., Davidson, I. (Eds.), Salt Tectonics, 100. Geological Society Special Publication, pp. 89–109.

Vernant, Ph., Nilforoushan, F., Hatzfeld, D., Abbassi, M.R., Vigny, C., Masson, F., Nankali, H., Martinod, J., Ashtiani, A., Bayer, R., Tavakoli, F., Chery, J., 2004. Present-day crustal deformation and plate kinematics in the Middle East constrained by GPS measurements in Iran and northern Oman. Geophysical Journal International 157, 381–398.

Walpersdorf, A., Hatzfeld, D., Nankali, H., Tavakoli, F., Nilforoushan, F., Tatar, M., Vernant, P., Chery, J., Masson, F., 2006. Difference in the GPS deformation pattern of North and Central Zagros (Iran). Geophysical Journal International 167, 1077–1088.

Weijermars, R., Jackson, M.P.A., Vendeville, B.C., 1993. Rheological and tectonic modeling of salt provinces. Tectonophysics 217, 143–174.

Whitaker, A.E., Bartholomew, M.J., 1999. Layer parallel shortening: a mechanism for determining deformation timing at the junction of the central and southern Appalachians. American Journal of Science 299, 238–254.

Williams, R.B.G., Swantesson, J.O.H., Robinson, D.A., 2000. Measuring rates of surface downwearing and mapping microtopography: The use of micro-erosion meters and laser scanners in rock weathering studies. Zeitschrift für Geomorphologie N.F. Vol. 120 (Suppl.), 51–66.